www.sciencemag.org/content/342/6158/617/suppl/DC1

Supplementary Materials for

Pacific Ocean Heat Content During the Past 10,000 Years

Yair Rosenthal,* Braddock K. Linsley, Delia W. Oppo

*Corresponding author. E-mail: rosentha@imcs.rutgers.edu

Published 1 November 2013, *Science* **342**, 617 (2013)
DOI: 10.1126/science.1240837

This PDF file includes:

SUPPLEMTARY MATERIAL

Pacific Ocean Heat Content during the past 10,000 years

Yair Rosenthal[1*], Braddock K. Linsley[2] and Delia W. Oppo[3]

1. Makassar Strait Hydrography

The Makassar Straits between Borneo and Sulawesi, serves as a major conduit for the Indonesian Throughflow (ITF) transporting water from the Pacific to the Indian Ocean (Fig S1, S2) primarily through the main thermocline (~150-400m; (*1*). Annual sea surface temperatures (SST) at this region is on average 29.3°C with coldest SST occurring from July to September (JAS) during the upwelling season (*2*). Surface salinity in this region varies temporally and spatially following the rainy and dry seasons. Below the surface, water in the upper thermocline represents a mixture of North Pacific and to a lesser extent south Pacific subtropical waters (NPSW and SPSW, respectively), which is recognized as salinity maximum between 100 and 200 m (Fig. S3, S4). Within he main thermocline, between about 200 and 500 m the inflow of low salinity North Pacific Intermediate Water (NPIW) dominates the ITF flow, recognized by its salinity minimum (~ 34.45 psu; 26.5 σ_θ). Salinity increases below the main thermocline (at ~450m) and remains relatively constant down to 1000m (~34.55 psu; 27.2-27.3 σ_θ). This water mass known as the Indonesian Intermediate Water (IIW) is formed in the Banda Sea by strong vertical mixing between shallow/warm/relatively fresh and deep/cold/relatively salty waters (*1, 3*). We note that the intermediate water exchange through the Makassar Strait is restricted, however, below ~680 m by the Dewakang Sill on the southern edge of the straits (*1, 4*). Therefore, our deep cores (>650) m in the Flores Sea, south of the sill, are all influenced by IIW forming in the Banda Sea.

2. Age models

Accelerator mass spectrometry (WHOI AMS facility) ^{14}C dates were obtained on mixed planktonic species (primarily *G. ruber* and *G. sacculifer*) and corrected and converted to calendar age (*5*) using a reservoir age correction of 500 years for all the cores (*6*) (Table S1). In core 13GGC we identified an ash layer at 3 cm depth, which we assumed to be Mt. Tambora ash layer, and therefore assigned this depth the age of the last eruption 1815 CE.

We generated several high-resolution records of the Common Era (CE) using a combination of multi- and gravity cores. The composite records have higher resolution and more replication than the longer ones. The age models for the gravity cores are based on AMS radiocarbon dating. The chronology of the multi-cores is based on several criteria. All multi-core tops contained sigifivant amounts of bomb radiocarbon. Therefore, we use the similarity between the planktonic foraminiferal $\delta^{13}C$ records and the decrease in atmospheric $\delta^{13}C$ (aka Suess Effect) to date the top-most part of the multi cores, whereas AMS radiocarbon dating was used to determine the age of the bottom of the multi-cores. We assume a linear age change between the top and bottom, and tested this assumption using lead isotopes (^{210}Pb) dating and correlation of distinctive ash layers in these cores with known historic volcanic eruptions (e.g., Mt Tambora's eruption in 1815). For details see MSc thesis by Katharine L. Esswein (*7*).

3. Analytical methods

For Mg/Ca analysis, foraminiferal tests were cleaned using a protocol to remove clays, metal oxides and organic matter following the protocol of (*8*) as modified by (*9*). The foraminifera were gradually dissolved in trace metal clean 0.065N HNO_3 (OPTIMA®) and 100μl of this solution was diluted with 300μl trace metal clean 0.5N HNO_3 to obtain a Ca concentration of 3±1 mmol L^{-1}. Samples were analyzed by Finnigan MAT ElementXR Sector Field Inductively Coupled Plasma Mass Spectrometer (ICP-MS) operated in low resolution ($m/\Delta m$=300) following the method outlined in (*10*). Fe/Ca and Al/Ca were used to monitor for sedimentary contamination. Direct determination of elemental ratios from intensity ratios requires control of the sample Ca concentration; in each run six standard solutions with identical elemental ratios but variable Ca concentrations, which covered the range of Ca concentrations of the samples, were included. These solutions allowed us to quantify and correct for the effects of variable Ca concentrations in a sample solution on the accuracy of Mg/Ca measurement (so-called matrix effects) based on the sample's Ca concentration (*10*). Matrix corrections were typically <0.1 mmol mol^{-1} Mg/Ca. Instrument precision was determined by repeated analysis of three consistency standards over the course of this study. The long term precision of the consistency standard with Mg/Ca of 1.10 mmol mol^{-1} was ±1.5% (r.s.d.), the precisions of the consistency standards with Mg/Ca of 2.40 mmol mol^{-1} and 6.10 mmol mol^{-1} was about ±1.2%.

Isotope measurements were done both at Woods Hole Oceanographic Institution (using a Kiel device coupled to a Finnigan MAT 251 mass spectrometer) and at the State University of New York at Albany (using a Fisons Optima mass spectrometer). The long-term external precision of $\delta^{18}O$ analysis was 0.07‰ and 0.05‰ at WHOI and SUNYA, respectively.

4. Intermediate Water Temperature estimates

Intermediate water temperature (IWT) reconstructions are based on Mg/Ca measurements in the benthic foraminifer *Hyalinea balthica* and the recently published calibration [Mg/Ca=(0.488±0.03)xBWT] (*11, 12*). The $\delta^{18}O$ records are based mostly on measurements of *H. balthica* tests and supplemented when its abundance was low, with additional data from *Cibiciodes pachyderma* (Fig. S3). For both species, measured $\delta^{18}O$ data were adjusted by +0.64‰ to calculate the equilibrium value of calcite (*11*). Previous work showed that core top Mg/Ca-derived temperatures and $\delta^{18}O$ ratios of *H. balthica* tests reliably reflect bottom water temperatures (BWTs) at the studied sites (*11*). We note, however, that temperature estimates for our deepest core (900 m) are slightly higher than expected, which may reflect the fact that its depth is at the lower limit of the ecological tolerance of this species.

5. Errors in temperature estimates

The calibration data and a validation test of (*11*) demonstrates that the uncertainty in reconstructing the absolute intermediate water temperature (IWT) and salinity from paired Mg/Ca and $\delta^{18}O$ measurements of *H. balthica* is better than ±0.7°C and ±0.69 units, respectively and for density better than better than 0.3σ_θ units. However, the error in reconstructing relative, rather than absolute, changes in IWT is much smaller, on the order of about 0.045° and 0.09°K for 67 and 95% confidence (1SEE and 2SEE). The error associated with the instrumental analysis is about the same i.e. 0.09°K. A larger error comes from variability among samples at the same depth interval. Replicated measurements of parallel samples at the same depth interval of a core and comparison of data generated from cores bathed under the same water mass suggest a SD in down core records of ~0.35°K. In generating the compiled records shown in figure 2 and 3 we estimated the standard deviations (1SD) in the records as follows:

1) At 500 meters we have only one record, so we estimate the $SD=(0.09)^2+(0.09)^2+(0.35)^2=0.37°$

To calculate the SEE we used 3-point moving average which results in a smaller uncertainty of the relative change of $1\text{-}SEE=(0.09)^2+(0.09)^2+(0.35/\text{sqrt}(2))^2=0.35°$ (using 1 degree of freedom)

2) At 600-900 meters we have three records. The estimated SD is the same as above $SD=(0.09)^2+(0.09)^2+(0.35)^2=0.37°$

To calculate the SEE we re-sampled the three records at constant time intervals and averaged the results. The uncertainty of the relative change is $1\text{-}SEE=(0.09)^2+(0.09)^2+(0.35/\text{sqrt}(2))^2=0.35°$

6. Correcting IWT for sea level change

The 30m sea level rise from the early to late Holocene should have only minor effect on our IWT estimates, because our cores are at the bottom of the thermocline where the temperature gradient is very low. We use the Barbados sea level record (*13*) and the modern thermocline structure to estimate this bathymetric influence. We estimate that the early-mid Holocene IWT estimates are at most overestimated by 0.2-0.4°C relative to the true climatologic change due to the lower sea level at that time.

7. Surface and upper Thermocline Temperature estimates

In this paper we use the published sea surface (SST) and upper Thermocline Water (TWT) temperature reconstructions. SST records are based on Mg/Ca ratios in the mixed-layer foraminifer *G. ruber s.s.* (white variety 212-300 µm size). Upper thermocline temperature (TWT) reconstructions are based on Mg/Ca measurements in the subsurface planktonic foraminifer *P. obliquiloculata*. Modern calibrations suggest that in the IPWP region *P. obliquiloculata* tends to calcify at about 75-100m depth(*14, 15*). We treat the records as strictly reflecting changes in TWT, as was done in the original publications, although it is difficult to rule out that changes in calcification depth partially contributed to the observed changes.

8. Estimating down-core salinity

The $\delta^{18}O$ composition of sea water was calculated from the sea-level corrected $\delta^{18}O_{sw}$ records using the equation of $\delta^{18}O_{sw}$(‰SMOW)=0.27+(T-16.9+4* $\delta^{18}O_{calcite}$ (‰PDB))/4 (*16*), where T is temperature in °C after adjusting the measured benthic foraminifera $\delta^{18}O_{calcite}$ by +0.64‰. Seawater salinities for the deep sites at 500, 600 and 650 m were then estimated using available data from three hydrographic stations intersecting the NPIW and AAIW water masses, closest to our region (Table S2). One station is from the western Pacific (29.08°N 142.85°E; 0-1000m) from Oba (1988) (*17*). The other stations are located in the southern hemisphere intersecting AAIW (39.95°S 109.97°E and 19.49°S 109.97°E; 0-1400 m). Using this data set we generate the following relationship:

$\delta^{18}O_{sw\text{-}iv}$(‰SMOW)=0.74*Salinity – 25.4 (r^2=0.9), where $\delta^{18}O_{sw\text{-}iv}$ is the ice-volume corrected $\delta^{18}O_{sw\text{-}iv}$ using the Barbados sea level record (*13*). We prefer this relationship over published ones from the western equatorial Pacific since the latter are based on surface water measurements, which are both very variable in the tropical Pacific and do not reflect the intermediate water.

Although we are fully aware of potential errors associated with the conversion of $\delta^{18}O_{sw\text{-}iv}$ into salinity estimates, it is instructive to assess the down core variations in the density of these water masses. Plotting the down-core data on a T-S plot allows for a visual assessment of down core trends in water mass densities and provides important insights as to the likely processes that affect T & S changes in our records, in a way that cannot be gained by looking at the primary records. Core top estimates fall somewhat off the modern CTD data, but nonetheless agree within the 2SE of the estimate.

9. Pacific Ocean Heat Content (OHC) estimates

We use the compiled IWT anomaly records to estimate the Pacific OHC at four time slices: 1) Early Holocene 9000-7500 years BP; 2) mid-Holocene 5000-3000 years BP; 3) 0-1000 CE which includes the Medieval Warm Period; 4) 1400-1800 CW which includes the Little Ice Age. First we combined the ΔIWT records presented in figures 2 & 3 and resampled at 200 years resolution using linear integration between samples. We then calculate the OHC for the 0-700m depth interval using the following equation:

$$OHC(t)= OHC(t-\Delta t)+C_p*M_z*\Delta T$$

where OHC(t) is the Ocean Heat Content (in Joules) at each time step, Δt= 200 years intervals, Cp is the seawater heat content (4000 Joules/°C/kg), M_z is the seawater mass at the specified water volume (in Kg) and ΔT is the temperature change during each time interval. To compare our estimates with modern observations we normalize the records to a common reference period. The top age of our composite & smoothed Pacific IWT record is ~1970 CE. Since our core top IWT estimates are consistent, within errors, with the hydrographic data we normalize our OHC record to this reference period. The Pacific OHC for the 0-700m depth changed between $-2x10^{22}$ J and 0 between 1955 and 1995 (http://www.nodc.noaa.gov/OC5/3M_HEAT_CONTENT/)(*18*). Thus we normalized our OHC reconstruction to $-1x10^{22}$ J to match the top samples with the observed OHC during the 1965-1970 CE period.

There are significant uncertainties in this estimation of which the largest is about the volume of water affected by the IWT changes. With no additional benthic Mg/Ca records it is difficult to assess the oceanographic extent of the observed IWT changes. Instrumental observations show regional variability in OHC changes in the Pacific Ocean, with reduced warming in the central and eastern tropical Pacific as compared with the western Pacific. This pattern may apply only for short-term, transient changes and on longer time scales the change may be more uniform over the entire Pacific when the upper ocean is equilibrated with the atmosphere warming. But, it is also plausible that dynamical responses in the tropical Pacific associated with zonal changes in the depth of the equatorial thermocline resulted in regional differences in the magnitude of OHC changes between the western and eastern Pacific. To account for the different scenarios we consider three sensitivity cases:

Case 1) Assumes that IWT trends observed in Indonesia apply to most of the Pacific volume (75%) between 0-700m (100% M_z= 1.12x10^{20} kg; http://ngdc.noaa.gov/mgg/global/etopo1_ocean_volumes.html).

Case 2) Assumes that IWT trends observed in Indonesia apply to 50% of the Pacific volume between 0-700m.

Case 3) Assumes that IWT trends observed in Indonesia apply to 25% of the Pacific volume between 0-700m.

The minimum case (25%) assumes the observed trends affected only the western Pacific, whereas the central and eastern Pacific were unaffected. However, there are some indications that these changes might have extended into the eastern Pacific Ocean. Benthic foraminifera δ^{18}O records from the Santa Barbara Basin (ODP site 893A at 580m) (*19*), California Margin (ODP Site 1017E at 956m) (*20*) and North Pacific (*21*) show minimum values at the early Holocene with subsequent trend of 0.1-0.15‰ toward heavier values in the late Holocene. Although we cannot unequivocally attribute these trends to cooling, we note that they are consistent with the trend observed in our 70GGC record suggesting that changes observed in Indonesia might have affected the entire Pacific intermediate water mass. This would be consistent with the expectation that on centennial and longer time scales the ocean should be in thermal equilibrium with the atmosphere (*18, 22*). It is also noteworthy that changes in the surface layer contribute very little to the OHC (<<10% in modern observations) (*18*) and therefore, the fact that Holocene SST changes are small doesn't introduce a large error to the estimates.

For each of the cases we also estimate the rate of OHC change for three intervals during the Holocene and Common Era when significant changes in OHC occur and compare these with modern rates (Table S3). First, we define multi-centennial temperature trends (Fig. S7) for the three time intervals namely a) mid Holocene transition 2 – 7.5 Ka; B) MWP to LIA transition 1100-1700 CE; and C) LIA to present 1600 – 1950 CE. We then estimate the rate of OHC change considering 25, 50, 75% of the Pacific -700m volume. In these estimates we also include the errors associated with our IWT estimates. We compare these rates with the average rate estimated for the 1955-2010 period for the Pacific Ocean. Using the total temperature change in each interval we calculate the change in OHC for each time interval and the rate of change in Joules per century. The estimates in Table S3, albeit with large uncertainties, suggest that the modern rate of Pacific OHC change is significantly higher than the absolute rates reconstructed for the past. This is the case even when considering the maximum ΔIWT rate (-0.15°K per century) from the MWP to LIA (~1100-1700 CE) for 75% volume.

References

1. A. Gordon, Oceanography of the Indonesian Seas and their throughfow. *Oceanography* **18**, (2005).
2. T. M. Smith, R. W. Reynolds, T. C. Peterson, J. Lawrimore, Improvements to NOAA's historical merged land-ocean surface temperature analysis (1880-2006). *J. . Climate* **21**, 2283 (2008).
3. L. D. Talley, J. Sprintall, Deep expression of the Indonesian Throughflow: Indonesian Intermediate Water in the South Equatorial Current. *J. Geophys. Res.* **110**, (2005).
4. R. A. Fine, R. Lukas, F. M. Bingham, e. al., The western equatorial Pacific: A water mass crossroads. *J. Geophys. Res.* **99**, 25 (1994).
5. R. G. Fairbanks, e. al., Marine radiocarbon calibration curve spanning 0 to 50,000 years B.P. based on paired 230Th/234U/238U and 14C dates on pristine corals. . *Quat. Sci. Rev.* **24**, 1781 (2005).
6. J. Southon, M. Kashgarian, M. Fontugne, B. Metiver, W. W. S. Yim, Marine reservoir corrections for the Indian Ocean and Southeast Asia. . *Radiocarbon* **44**, 167 (2002).
7. K. Esswein, Rutgers, The State University of New Jersey (2012), 50 pages.
8. E. A. Boyle, L. D. Keigwin, Comparison of Atlantic and Pacific paleochemical records for the last 250,000 years: changes in deep ocean circulation and chemical inventories. *Earth Planet. Sci. Lett.* **76**, 135 (1985).
9. Y. Rosenthal, E. A. Boyle, L. Labeyrie, Last glacial paleochemistry and deep water circulation in the Southern Ocean: Evidence from foraminiferal cadmium. *Paleoceanography* **12**, 778 (1997).
10. Y. Rosenthal, F. Field, R. M. Sherrell, Precise determination of element/calcium ratios in calcareous samples using Sector Field Inductively Coupled Plasma Mass Spectrometry. *Analytical Chemistry* **71**, 3248 (1999).
11. Y. Rosenthal *et al.*, Temperature calibration of Mg/Ca ratios in the intermediate water benthic foraminifer Hyalinea balthica. *Geophys. Geochem. Geosys* **12**, doi:10.1029/2010GC003333 (2011).

12. A. Morley *et al*., Climate variability and signal propagation via North Atlantic central water formation during the Late Holocene. *Earth Planet. Sci. Lett.* **308**, 161 (2011).
13. R. G. Fairbanks, A 17,000-year glacio-eustatic sea level record: influence of glacial melting rates on the Younger Dryas event and deep-ocean circulation. *Nature* **342**, 637 (1989).
14. M. Mohtadi *et al*., Reconstructing the thermal structure of the upper ocean: Insights from planktic foraminifera shell chemistry and alkenones in modern sediments of the tropical eastern Indian Ocean. *Paleoceanography* **26**, (2011).
15. J. Xu, A. Holbourn, W. Kuhnt, Z. Jian, H. Kawamura, Changes in the thermocline structure of the Indonesian outflow during Terminations I and II. *Earth and Planetary Science Letters* **273**, 152 (2008).
16. N. J. Shackleton, Attainment of isotopic equilibrium between ocean water and the benthonic foraminifera genus Uvigerina: Isotopic changes in the ocean during the last glacial. *Colloques Internationaux du C.N.R.S.* **219**, (1974).
17. T. Oba, in *Asian Marine Geology,* P. Wang, Q. Lao, Q. He, Eds. (China Ocean Press, Beijing, 1988), pp. 169-180, .
18. S. Levitus *et al*., World ocean heat content and thermosteric sea level change (0–2000 m), 1955–2010. *Geophys. Res. Lett.* **39**, 5 (2012).
19. J. P. Kennett, e. al., Quaternary Interstadials Carbon Isotopic Evidence for Methane Hydrate Instability During Quaternary. *Science* **288**, 128 (2000).
20. J. P. Kennett, e. al., Eds., Latest Quaternary paleoclimatic and radiocarbon chronology, Hole 1017E, Southern California margin, (2000).
21. J. C. Herguera, e. al., Intermediate and deep water mass distribution in the Pacific during the Last Glacial Maximum inferred from oxygen and carbon stable isotopes. *Quaternary Science Reviews* **29**, 1228.
22. J. Hansen, e. al., Earth's Energy Imbalance: Confirmation and Implications. *Science* **308**, 1431 (2005).
23. W. Zenk, et al., Pathways and variability of the Antarctic Intermediate Water in the western equatorial Pacific Ocean. *Progress in Oceanography* **67**, 245 (2005).
24. H. G. Ostlund, H. Craig, W. S. Broecker, D. W. Spencer, *GEOSECS Atlantic, Pacific, and Indian Ocean Expeditions, Vol. 7, Shorebased Data and Graphics.* (National Science Foundation, Washington, DC, 1987), pp. 200.
25. T. Oba, in *Asian Marine Geology,* P. Wang, Q. Lao, Q. He, Eds. (China Ocean Press, Beijing, 1988), pp. 169-180,

TABLES AND FIGURES

Table S1: Radiocarbon measurements made on mixed planktonic foraminifera at the National Ocean Sciences Accelerator Mass Spectrometry Facility (NOSAMS) and converted to calendar age using a reservoir age of 500 years (*5, 6*).

CORE	Depth	ID	^{14}C Age Years B.P.	S.D. Years	Calendar age Years B.P.	S.D. Years
MC6	43-44	OS-90418	745	30	286	53
7GGC	12-14	OS-90414	445	30	>Modern	-
7GGC	50-52	OS-79127	1293	20	702	16
7GGC	163-164	OS-90419	2210	35	1611	50
7GGC	200-202	OS-79128	2867	20	2355	16
7GGC	350-352	OS-79211	4323	20	4212	37
7GGC	448-449	OS-90417	5781	40	6038	69
10GGC	7-8	OS-45433	635	30	275	37
10GGC	160-161	OS-56409	3500	35	3385	58
10GGC	336-337	OS-56410	7890	50	8342	91
10GGC	488-489	OS-45434	10700	70	12050	63
13GGC	30-32	OS-57851	925	30	564	20
13GGC	100-101	OS-56281	2190	30	1784	42
13GGC	272-273	OS-56282	5050	40	5408	63
13GGC	408-409	OS-56408	8220	45	8730	40
13GGC	503-504	OS-45499	9610	60	10422	96
MC31	0-1	OS-45713	>Modern	-	-	-
MC31	26-27	OS-58731	620	30	138	94
MC31	49-50	OS-52863	675	45	232	95
32GGC	3.5-4.5	OS-52745	45	40	*	
32GGC	70.5-71.5	OS-57846	920	30	503	14
32GGC	135.5-136.5	OS-54078	1140	30	639	34
32GGC	179.5-180.5	OS-57776	1610	35	1034	44
32GGC	229.5-230.5	OS-54079	2210	30	1644	46
32GGC	275.5-276.5	OS-57777	2460	35	1928	38
34GGC	8.5-9.5	OS-52741	780	55	358	79
34GGC	103.5-104.5	OS-52742	1320	40	748	43
34GGC	199.5-200.5	OS-52743	1900	45	1320	30
34GGC	303.5-304.5	OS-52733	2270	45	1719	59
34GGC	380-381	OS-45717	2750	30	2308	43
47MC	58-60	OS-81572	1120	35	604	39
48GGC	20-22	OS-81571	1020	35	532	22
48GGC	60-62	OS-87066	1180	35	649	30

48GGC	100-102	OS-81693	1570	30	967	27
48GGC	140-142	OS-87074	2050	35	1428	47
48GGC	180-182	OS-81692	2280	35	1701	47
70GGC	63-64	OS-45435	1310	30	716	24
70GGC	104-105	OS-54152	2750	50	2274	68
70GGC	176-177	OS-54153	4240	50	4092	75
70GGC	201-202	OS-60747	4850	40	4894	53
70GGC	241-242	OS-60750	5410	35	5631	28
70GGC	280-281	OS-54154	6160	60	6435	65
70GGC	320-321	OS-60737	7190	45	7562	34
70GGC	361-362	OS-60748	10250	40	11191	25
70GGC	393-394	OS-65581	12550	50	13849	60
70GGC	405-406	OS-45436	12900	45	14265	114

Table S2: Seawater and salinity and $\delta^{18}O$ measurements used for determining the modern relationship in this region

Longitude	Latitude	Depth	pot T °C	Salinity	$\delta^{18}O$ ‰SMOW	Year	Ref
101.29	-19.49	472	9.57	34.78	0.2	1978	1
101.29	-19.49	638	7.07	34.57	0.09	1978	1
101.29	-19.49	808	6.02	34.64	0.09	1978	1
101.29	-19.49	1193	4.51	34.65	0.07	1978	1
142.85	29.08	0	28.3	34.67	0.06	1984	2
142.85	29.08	48	21.64	34.77	0.17	1984	2
142.85	29.08	97	18.83	34.82	0.16	1984	2
142.85	29.08	193	17.7	34.81	0.29	1984	2
142.85	29.08	290	16.51	34.79	0.19	1984	2
142.85	29.08	387	14.52	34.6	0.09	1984	2
142.85	29.08	483	11.76	34.4	-0.05	1984	2
142.85	29.08	677	6.16	34.08	-0.28	1984	2
142.85	29.08	967	3.85	34.31	-0.28	1984	2

1) GEOSECS Ostlund et al (1987)
2) Oba (1988)

Table S3: Estimated changes in Pacific ocean heat content (OHC). The three tables depict 3 different sensitivity tests associated with the uncertainties in the volume of the Pacific ocean involved in these changes and the SD in temperature estimates. Modern observations for the 1955-2010 C.E. are from Levitus et al. 2012 (http://www.nodc.noaa.gov/OC5/3M_HEAT_CONTENT/index3.html)

A. Pacific OHC estimate considers <u>50% Pacific volume and average temperature</u> changes inferred from Fig. 8

Period	**Observed ΔT °K**	**ΔHo 10^{22} Joules [c]**	**Δt years**	**ΔHo 10^{22} Joules/ century**	**ΔT °K/ century**
2-7.5 Ka B.P [a]	-1.1	-25	5500	-0.45	-0.02
1700-1100 CE [b]	-0.9	-20	600	-3.4	-0.15
1950-1600 CE	0.25	5.6	370	1.5	0.09
2010-1955 CE	***0.11***	***8.4***	***55***	***15***	***0.032***

B. Upper bound OHC estimate considers <u>75% Pacific volume and maximum temperature</u> changes (Avg+S.E.) inferred from Fig. 8

Period	**Observed ΔT °K**	**ΔHo 10^{22} Joules [c]**	**Δt years**	**ΔHo 10^{22} Joules/ century**	**ΔT °K/ century**
2-7.5 Ka B.P [a]	-1.4	-47	5500	-0.85	-0.02
1700-1100 CE [b]	-1.1	-37	600	-6.1	-0.15
1950-1600 CE	0.35	12	370	3.2	0.09
2010-1955 CE	***0.12***	***8.4***	***55***	***16***	***0.032***

C. Lower bound OHC estimate considers <u>25% Pacific volume and minimum temperature</u> changes inferred from Fig. 8

Period	**Observed ΔT °K**	**ΔHo 10^{22} Joules [c]**	**Δt years**	**ΔHo 10^{22} Joules/ century**	**ΔT °K/ century**
2-7.5 Ka B.P [a]	-0.8	-8.9	5500	-0.16	-0.02
1700-1100 CE [b]	-0.7	-7.8	600	-1.3	-0.15
1950-1600 CE	0.15	1.7	370	0.45	0.09
2010-1955 CE	***0.10***	***8.4***	***55***	***14***	***0.032***

[a-] Although SST in the WPWP shows only a small cooling trend through the Holocene, reconstructed upper thermocline temperature trend is of similar magnitude as obtained for the BWT. Based on the modern data from (*18*) the contribution of the 0-100m surface layer to the Pacific OHC between 0 and 700 m is << 10%. During the Common Era, temperature changes at the surface and below 0-700 m are very similar suggesting uniform cooling of the 0-700m water column.

[b-] Considering Pacific ocean mass between 0-700m of $M_0=1.12\times10^{20}$kg (http://ngdc.noaa.gov/mgg/global/etopo1_ocean_volumes.html) and seawater heat capacity = 4000 J/°C/kg

SOM Figure captions

Figure S1: A map showing the annually averaged salinity distribution at 500m in the western equatorial Pacific. The main flow of the ITF through the main thermocline is shown by the black arrow-line. The main pathway of intermediate water into the Indonesian archipelago is through the New Guinea Coastal Undercurrent (NGCUC) shown in blue arrows. Recent studies suggest that the NGCUC gets a significant contribution from Antarctic Intermediate Water (AAIW). Part of the NGCUC spreads into the Banda Sea through the Lifamatola and Makssar passages while some returns eastward with the Southern and Northern Intermediate Counter Currents (SICC / NICC, rspectively) (*23*). Red stars mark the general core locations of our cores in the Makassar Strait and Flores Sea. Yellow stars mark location of other cores discussed in the text (see Figure S2).

Figure S2: Location maps showing core sites discussed in this paper. The top panel (A) shows the genera location of the cores and yellow circles mark the location of *P. obliquiloculata* records (MD78, MD88, MD04) are shown in the top map. The area marked with the yellow square is showed in the bottom panel with the location of cores 31MC/32GGC, 34GGC, 47MC/48GGC and 70GGC in the Labini Channel; 6MC/7GGC, 10GGC and 13GGC in the Bali Basin of the Flores Sea.

Figure S3: A north-south salinity section (0-2000 m) compiled from the World Ocean Circulation Experiment P9 (north Pacific along 137°E) and P11 (south Pacific along 155°E) lines. Note that the low salinity tongue at ~600-900m depth on the northern side of Papua New Guinea. This is the core of the NGCUC which arguably is linked to the low salinity AAIW clearly seen south of PNG.

Figure S4: CTD profiles of temperature and salinity obtained near the core sites in the Flores Sea, Makssar Strait, Celebes Sea and Maluku Sea east of Halmahera during the BJ8-2003 cruise. The CTD profiles are color-coded and their location is given in the legend. The inset shows salinity and temperature profiles from stations in the north

Pacific (17°N 137°E) and south Pacific (18.5°S 154.5°E) along the transect used in Fig. S3 clearly showing the distinct signatures of NPIW and AAIW, respectively. The increase in salinity below ~400m in our stations suggests an increasing contribution of south Pacific intermediate waters at the deeper sites. Arrows mark the depths of Makassar Straits and Bali Basin cores and the bottom water temperatures at each core site.

Figure S5: $\delta^{18}O$ in benthic foraminifera in our Holocene records.

Figure S6: Down core temperature and salinity data from cores at 500 m (70GGC and at 600-650 (combined 10 and 13GGC) plotted on a T-S plot. For the 500 m depth the early-mid Holocene (10.5-6 Ka) and Late Holocene (6-0 Ka) data are marked with the red and dark grey diamonds, respectively. For the 600-650 m depth the early-mid Holocene (10.5-6 Ka) and Late Holocene (6-0 Ka) data are marked with the light grey and dark blue squares, respectively. Isopycnal surfaces (solid black lines) are marked by their σ_θ values. The records show a slight decreasing density trend through the Holocene suggesting that the relative large temperature trends should have been compensated by salinity.

Figure S7: Common Era benthic *H. balthica* records from sites in the Makassar Strait and Flores Sea spanning a depth range of ~500-900 m. A) Mg/Ca-derived IWT; B) Bottom water $\delta^{18}O_{sw-iv}$. Age models for the records are based on AMS C-14 dating (Table S1).

Figure S8: Average trends of BWT changes (in °K per kyr) calculated from the compiled data set (Fig. 2, 3) the time intervals of a) 2 – 7.5 Ka; B) 1100-1700 CE; and C) 1600 – 1950 CE. Note that in the text and Table S3 the trends are given as °K per century.

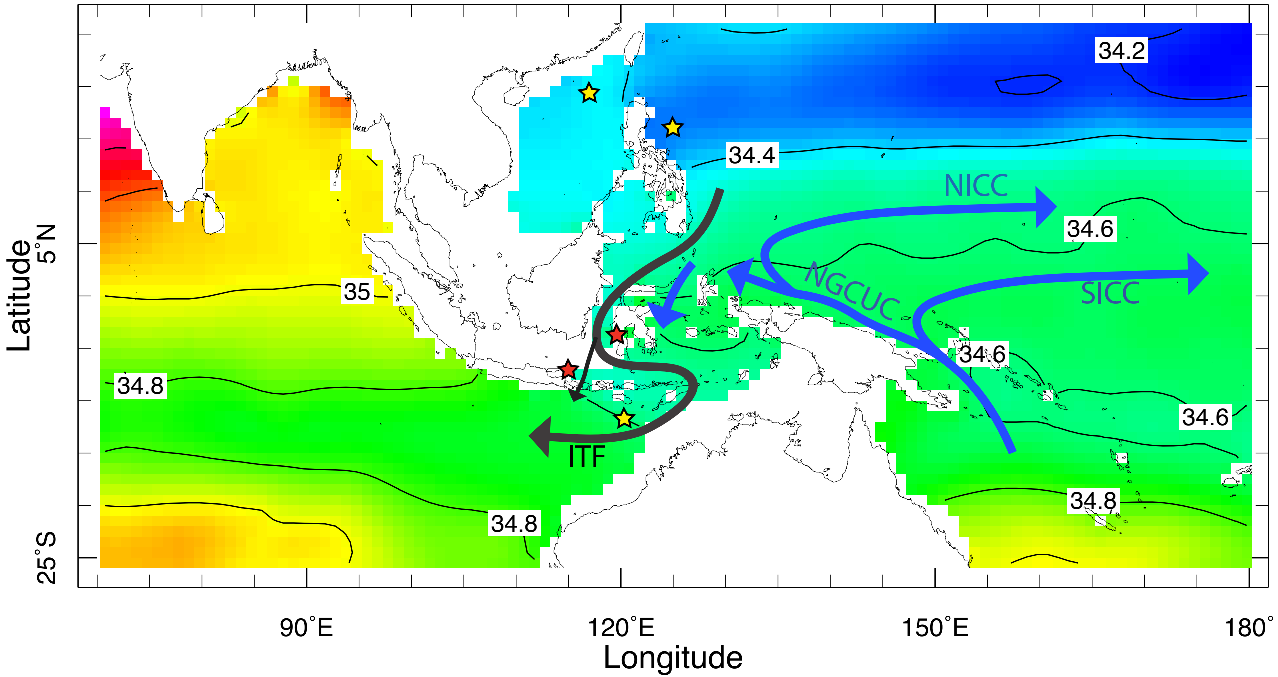

34.2
34.4
NICC
34.6
NGCUC
SICC
35
34.6
34.8
34.6
ITF
34.8
34.8
Latitude
5°N
25°S
90°E
120°E
150°E
180°
Longitude

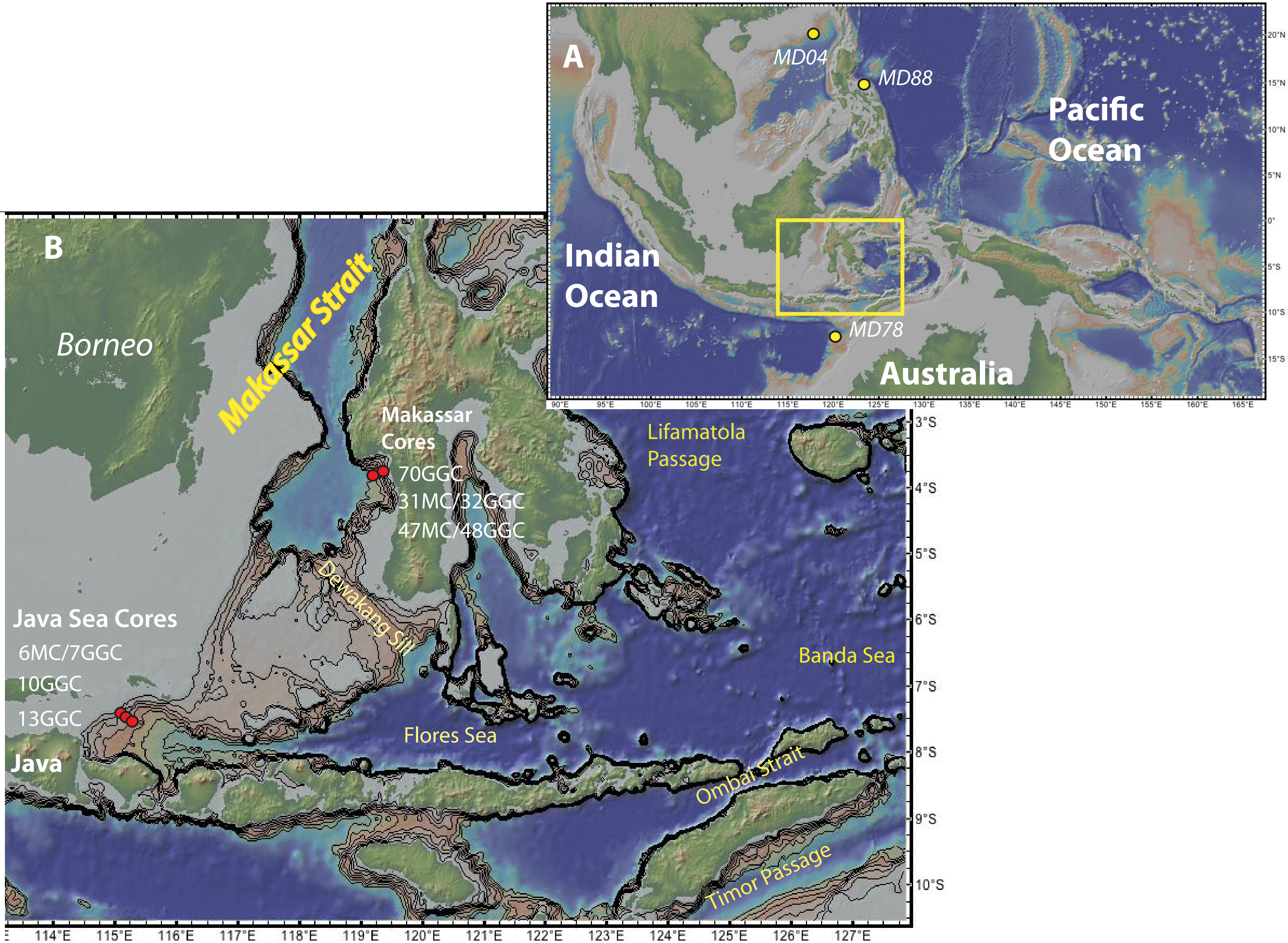
A
MD04
MD88
Pacific
Ocean
Indian
Ocean
MD78
Australia
B
Borneo
Makassar Strait
Makassar
Cores
70GGC
31MC/32GGC
47MC/48GGC
Lifamatola
Passage
Dewakang Sill
Java Sea Cores
6MC/7GGC
10GGC
13GGC
Java
Flores Sea
Banda Sea
Ombai Strait
Timor Passage
3°S
4°S
5°S
6°S
7°S
8°S
9°S
10°S
114°E
115°E
116°E
117°E
118°E
119°E
120°E
121°E
122°E
123°E
124°E
125°E
126°E
127°E

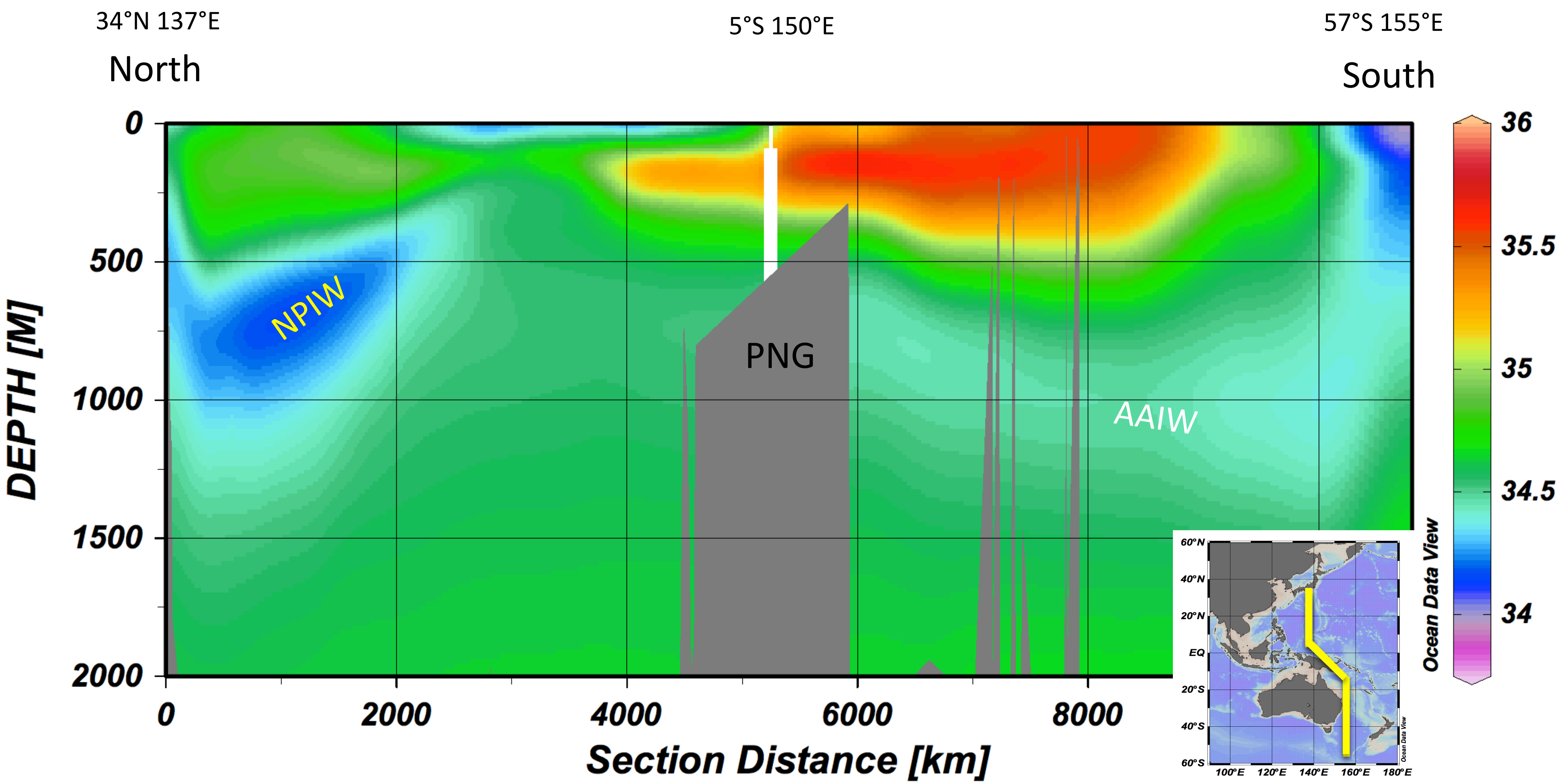
34°N 137°E
North
5°S 150°E
57°S 155°E
South
DEPTH [M]
0
500
1000
1500
2000
NPIW
PNG
AAIW
0
2000
4000
6000
8000
Section Distance [km]
36
35.5
35
34.5
34
Ocean Data View
60°N
40°N
20°N
EQ
20°S
40°S
60°S
100°E
120°E
140°E
160°E
180°E

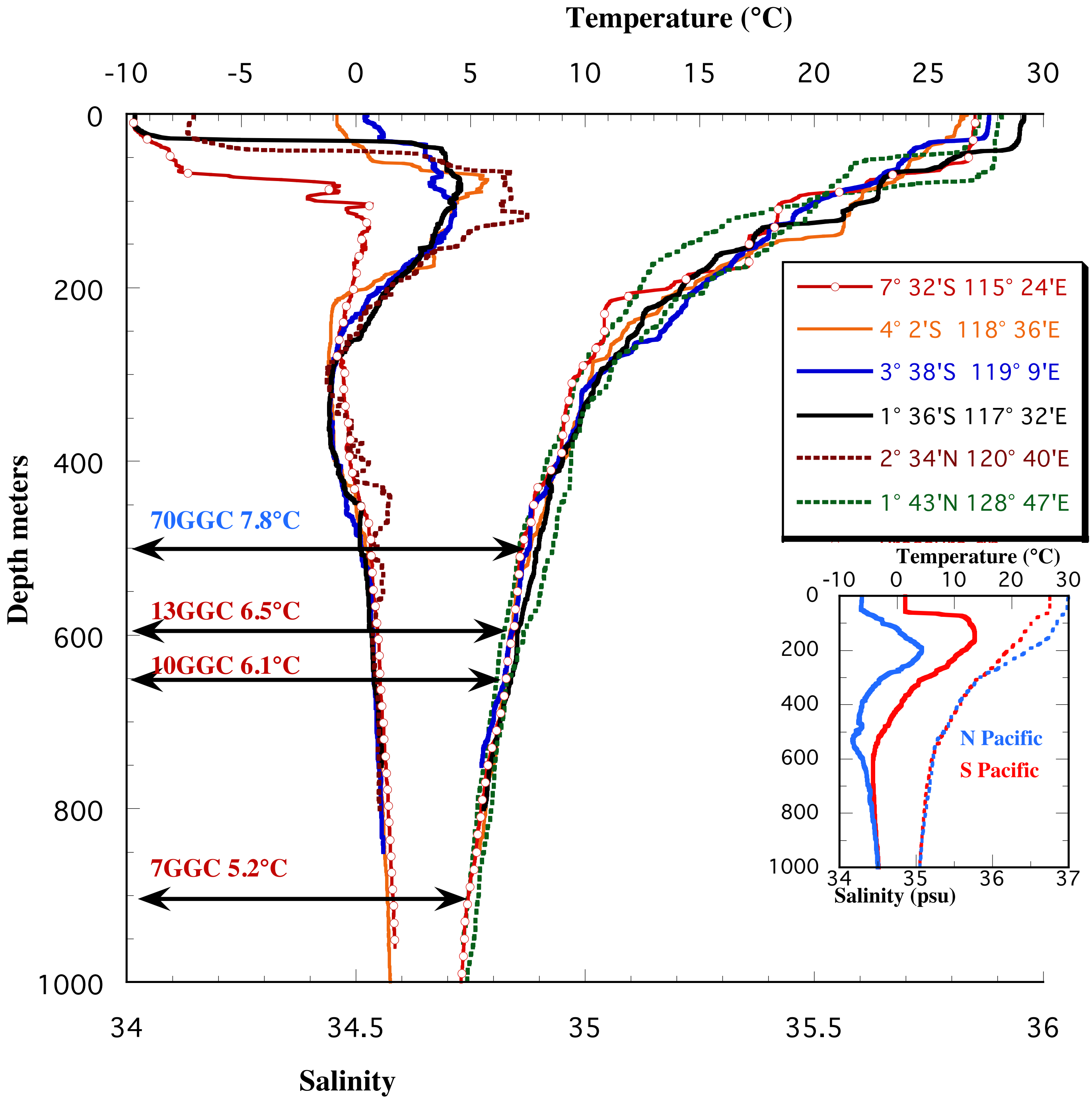

Temperature (°C)
-10
-5
0
5
10
15
20
25
30
0
200
400
600
800
1000
Depth meters
34
34.5
35
35.5
36
Salinity
7° 32'S 115° 24'E
4° 2'S 118° 36'E
3° 38'S 119° 9'E
1° 36'S 117° 32'E
2° 34'N 120° 40'E
1° 43'N 128° 47'E
70GGC 7.8°C
13GGC 6.5°C
10GGC 6.1°C
7GGC 5.2°C
Temperature (°C)
-10
0
10
20
30
0
200
400
600
800
1000
N Pacific
S Pacific
34
35
36
37
Salinity (psu)

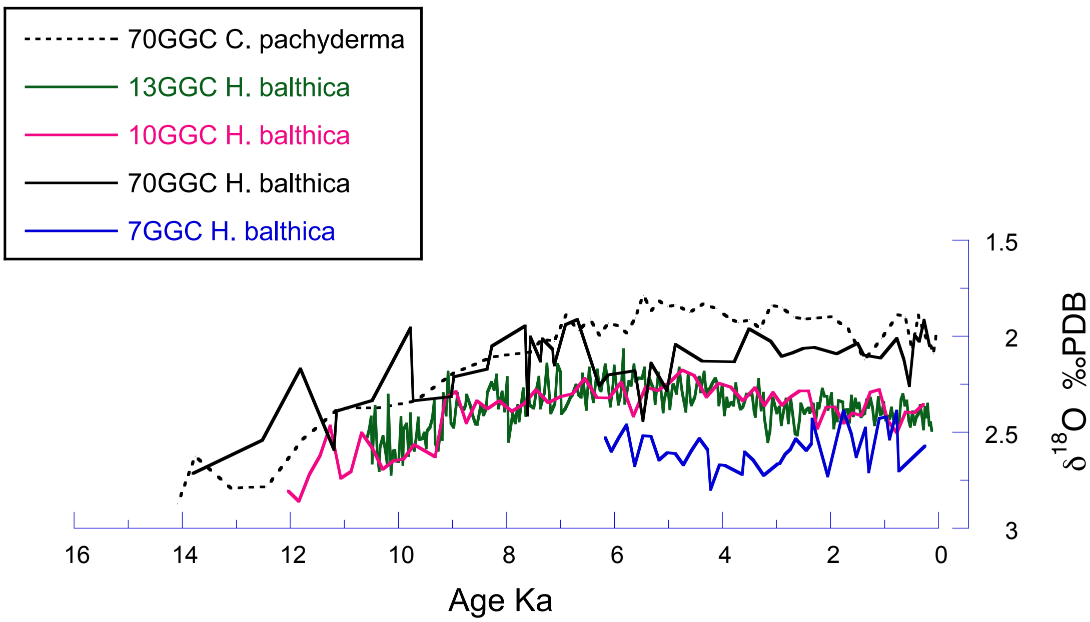
70GGC C. pachyderma
13GGC H. balthica
10GGC H. balthica
70GGC H. balthica
7GGC H. balthica
1.5
2
2.5
3
$\delta^{18}O$ ‰PDB
16
14
12
10
8
6
4
2
0
Age Ka

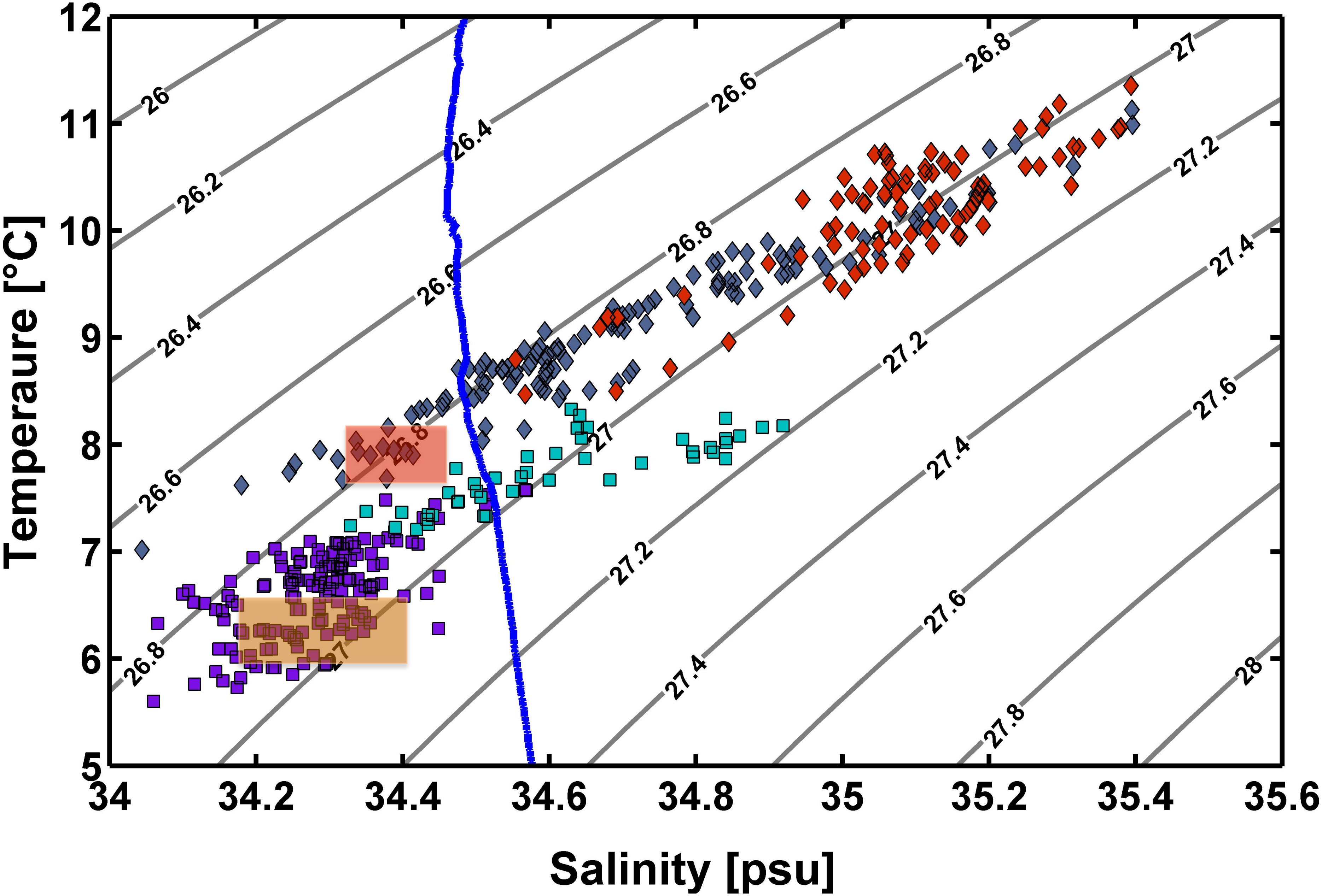

Temperaure [°C]
Salinity [psu]
12
11
10
9
8
7
6
5
34
34.2
34.4
34.6
34.8
35
35.2
35.4
35.6
26
26.2
26.4
26.6
26.8
27
27.2
27.4
27.6
27.8
28

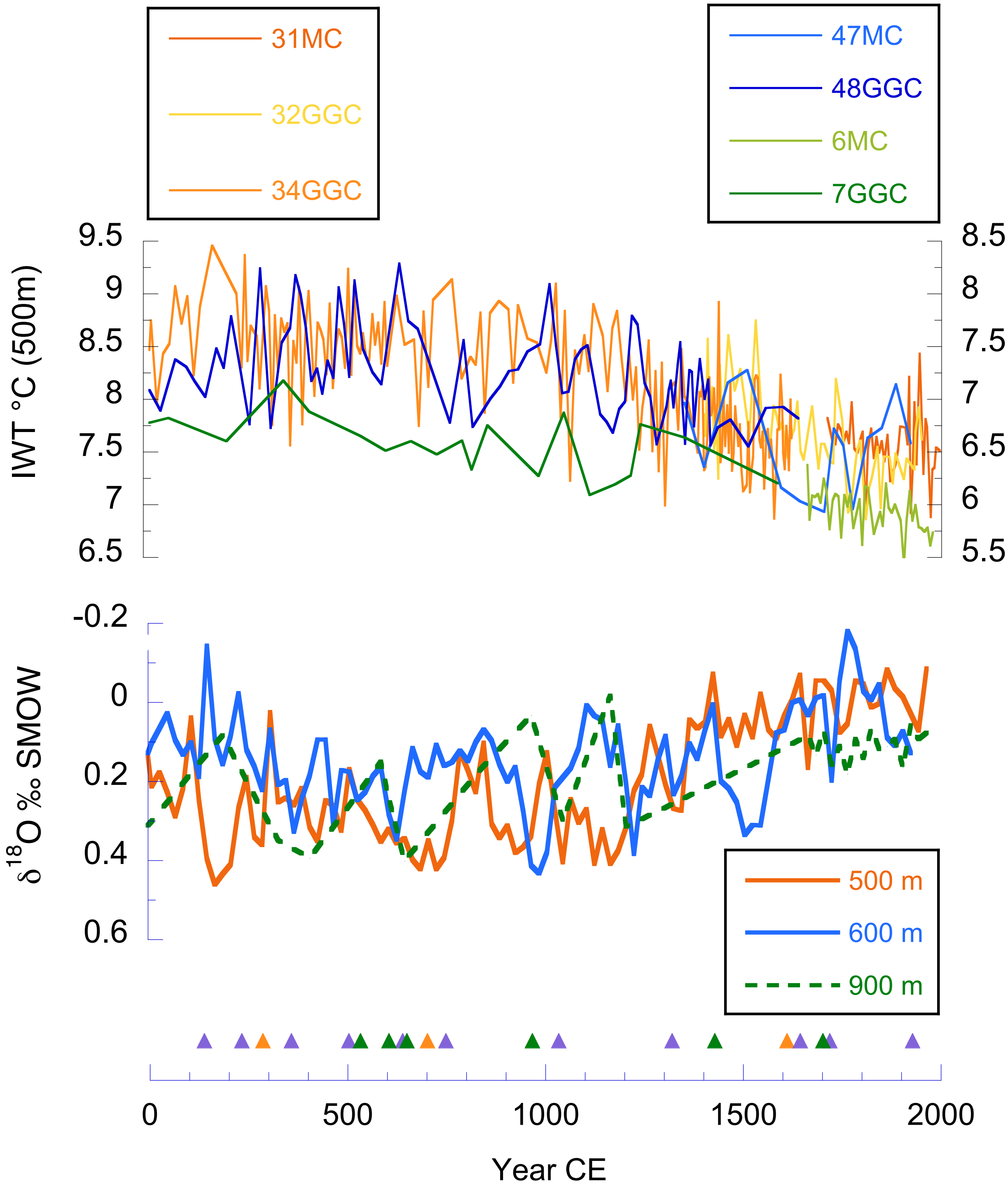

31MC
32GGC
34GGC
47MC
48GGC
6MC
7GGC
IWT °C (500m)
IWT °C (>500m)
9.5
9
8.5
8
7.5
7
6.5
8.5
8
7.5
7
6.5
6
5.5
$\delta^{18}O$ ‰ SMOW
-0.2
0
0.2
0.4
0.6
500 m
600 m
900 m
0
500
1000
1500
2000
Year CE

Fig. S8a

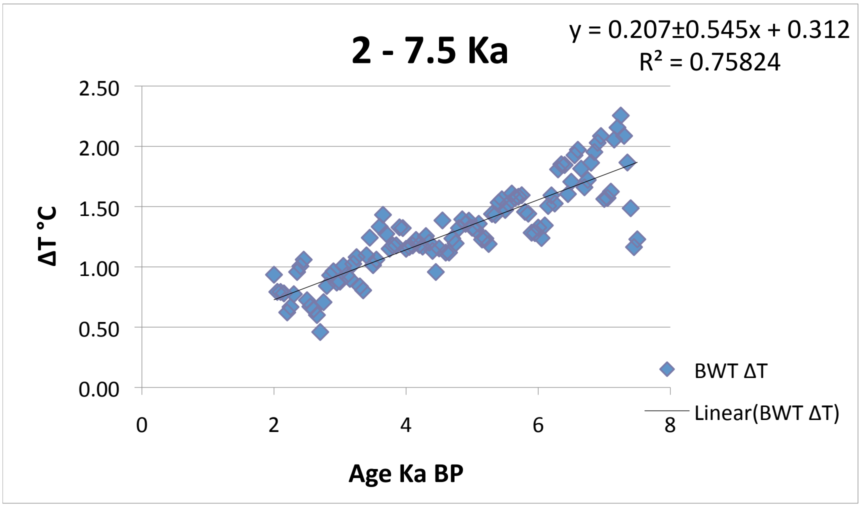

Fig. S8b

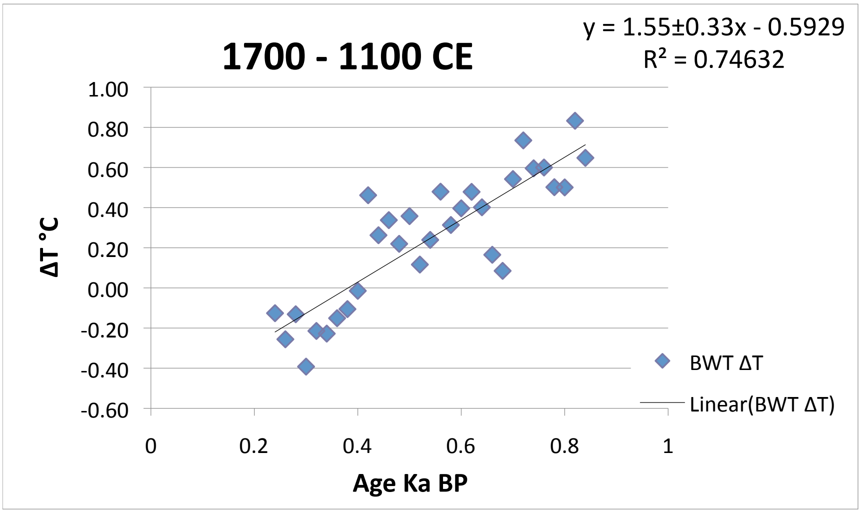

Fig. S8c

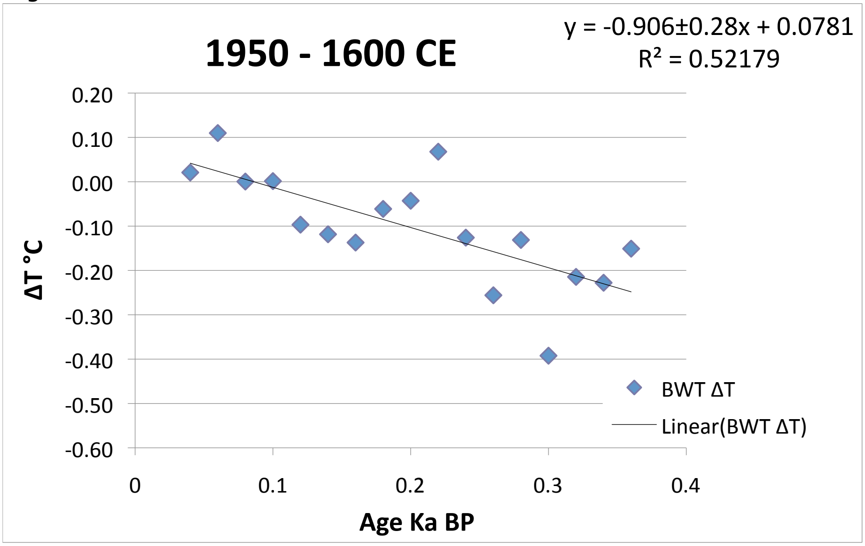

References and Notes

1. H. Wanner, J. Beer, J. Bütikofer, T. J. Crowley, U. Cubasch, J. Flückiger, H. Goosse, M. Grosjean, F. Joos, J. O. Kaplan, M. Küttel, S. A. Müller, I. C. Prentice, O. Solomina, T. F. Stocker, P. Tarasov, M. Wagner, M. Widmann, Mid- to Late Holocene climate change: An overview. *Quat. Sci. Rev.* **27**, 1791–1828 (2008). doi:10.1016/j.quascirev.2008.06.013

2. L. Leduc, R. Schneider, J.-H. Kim, G. Lohmann, Holocene and Eemian sea surface temperature trends as revealed by alkenone and Mg/Ca paleothermometry. *Quat. Sci. Rev.* **29**, 989–1004 (2010). doi:10.1016/j.quascirev.2010.01.004

3. D. R. Easterling, M. F. Wehner, Is the climate warming or cooling? *Geophys. Res. Lett.* **36**, L08706 (2009). doi:10.1029/2009GL037810

4. S. Levitus, J. Antonov, T. P. Boyer, C. Stephens, Warming of the World Ocean. *Science* **287**, 2225–2229 (2000). doi:10.1126/science.287.5461.2225

5. S. Levitus, J. I. Antonov, T. P. Boyer, O. K. Baranova, H. E. Garcia, R. A. Locarnini, A. V. Mishonov, J. R. Reagan, D. Seidov, E. S. Yarosh, M. M. Zweng, World ocean heat content and thermosteric sea level change (0-2000 m), 1955-2010. *Geophys. Res. Lett.* **39**, L10603 (2012). doi:10.1029/2012GL051106

6. J. Hansen, L. Nazarenko, R. Ruedy, M. Sato, J. Willis, A. Del Genio, D. Koch, A. Lacis, K. Lo, S. Menon, T. Novakov, J. Perlwitz, G. Russell, G. A. Schmidt, N. Tausnev, Earth's energy imbalance: Confirmation and implications. *Science* **308**, 1431–1435 (2005). doi:10.1126/science.1110252

7. R. A. Fine, R. Lukas, F. M. Bingham, M. J. Warner, R. H. Gammon, The western equatorial Pacific: A water mass crossroads. *J. Geophys. Res.* **99**, 25063–25080 (1994). doi:10.1029/94JC02277

8. A. Gordon, Oceanography of the Indonesian Seas and their throughflow. *Oceanography* **18**, 14–27 (2005).

9. L. D. Talley, J. Sprintall, Deep expression of the Indonesian Throughflow: Indonesian intermediate water in the South Equatorial Current. *J. Geophys. Res.* **110**, C10009 (2005). doi:10.1029/2004JC002826

10. W. Zenk, G. Siedler, A. Ishida, J. Holfort, Y. Kashino, Y. Kuroda, T. Miyama, T. J. Müller, Pathways and variability of the Antarctic Intermediate Water in the western equatorial Pacific Ocean. *Prog. Oceanogr.* **67**, 245–281 (2005). doi:10.1016/j.pocean.2005.05.003

11. S. Wijffels, J. Sprintall, M. Fieux, N. Bray, The JADE and WOCE I10/IR6 Throughflow sections in the southeast Indian Ocean. Part 1: Water mass distribution and variability. *Deep Sea Res. Part II Top. Stud. Oceanogr.* **49**, 1341–1362 (2002). doi:10.1016/S0967-0645(01)00155-2

12. J. Sprintall, S. E. Wijffels, R. Molcard, I. Jaya, Direct estimates of the Indonesian Throughflow entering the Indian Ocean: 2004–2006. *J. Geophys. Res.* **114**, C07001 (2009). doi:10.1029/2008JC005257

13. Y. Rosenthal, A. Morley, C. Barras, M. Katz, F. Jorissen, G. J. Reichart, D. W. Oppo, B. K. Linsley, Temperature calibration of Mg/Ca ratios in the intermediate water benthic foraminifer *Hyalinea balthica*. *Geophys. Geochem. Geosys.* **12**, 1–17 (2011).

14. A. Morley, M. Schulz, Y. Rosenthal, S. Mulitza, A. Paul, C. Rühlemann, Solar modulation of North Atlantic central Water formation at multidecadal timescales during the late Holocene. *Earth Planet. Sci. Lett.* **308**, 161–171 (2011). doi:10.1016/j.epsl.2011.05.043

15. Supplementary materials are available on *Science* Online.

16. B. K. Linsley, Y. Rosenthal, D. W. Oppo, Holocene evolution of the Indonesian Throughflow and the western Pacific warm pool. *Nat. Geosci.* **3**, 578–583 (2010). doi:10.1038/ngeo920

17. M. Mohtadi, D. W. Oppo, A. Lückge, R. DePol-Holz, S. Steinke, J. Groeneveld, N. Hemme, D. Hebbeln, Reconstructing the thermal structure of the upper ocean: Insights from planktic foraminifera shell chemistry and alkenones in modern sediments of the tropical eastern Indian Ocean. *Paleoceanography* **26**, PA3219 (2011). doi:10.1029/2011PA002132

18. J. Xu, A. Holbourn, W. Kuhnt, Z. Jian, H. Kawamura, Changes in the thermocline structure of the Indonesian outflow during terminations I and II. *Earth Planet. Sci. Lett.* **273**, 152–162 (2008). doi:10.1016/j.epsl.2008.06.029

19. S. Steinke, C. Glatz, M. Mohtadi, J. Groeneveld, Q. Li, Z. Jian, Past dynamics of the East Asian monsoon: No inverse behaviour between the summer and winter monsoon during the Holocene. *Global Planet. Change* **78**, 170–177 (2011). doi:10.1016/j.gloplacha.2011.06.006

20. H. Dang, Z. Jian, F. Bassinot, P. Qiao, X. Cheng, Decoupled Holocene variability in surface and thermocline water temperatures of the Indo-Pacific Warm Pool. *Geophys. Res. Lett.* **39**, 1–5 (2011).

21. V. Masson, F. Vimeux, J. Jouzel, V. Morgan, M. Delmotte, P. Ciais, C. Hammer, S. Johnsen, V. Y. Lipenkov, E. Mosley-Thompson, J.-R. Petit, E. J. Steig, M. Stievenard, R. Vaikmae, Holocene climate variability in Antarctica based on 11 ice-core isotopic records. *Quat. Res.* **54**, 348–358 (2000). doi:10.1006/qres.2000.2172

22. P. A. Mayewski, E. E. Rohling, J. Curt Stager, W. Karlén, K. A. Maasch, L. David Meeker, E. A. Meyerson, F. Gasse, S. van Kreveld, K. Holmgren, J. Lee-Thorp, G. Rosqvist, F. Rack, M. Staubwasser, R. R. Schneider, E. J. Steig, Holocene climate variability. *Quat. Res.* **62**, 243–255 (2004). doi:10.1016/j.yqres.2004.07.001

23. H. C. Bostock, T. T. Barrows, L. Carter, Z. Chase, G. Cortese, G. B. Dunbar, M. Ellwood, B. Hayward, W. Howard, H. L. Neil, T. L. Noble, A. Mackintosh, P. T. Moss, A. D. Moy, D. White, M. J. M. Williams, L. K. Armand, A review of the Australian–New Zealand sector of the Southern Ocean over the last 30 ka (Aus-INTIMATE project). *Quat. Sci. Rev.* **74**, 35–57 (2013). doi:10.1016/j.quascirev.2012.07.018

24. S. A. Marcott, J. D. Shakun, P. U. Clark, A. C. Mix, A reconstruction of regional and global temperature for the past 11,300 years. *Science* **339**, 1198–1201 (2013). doi:10.1126/science.1228026

25. C. Mauritzen, A. Melsom, R. T. Sutton, Importance of density-compensated temperature change for deep North Atlantic Ocean heat uptake. *Nat. Geosci.* **5**, 905–910 (2012).

26. D. W. Oppo, Y. Rosenthal, B. K. Linsley, 2000-year-long temperature and hydrology reconstructions from the Indo-Pacific warm pool. *Nature* **460**, 1113–1116 (2009). Medline doi:10.1038/nature08233

27. M. E. Mann, Z. Zhang, M. K. Hughes, R. S. Bradley, S. K. Miller, S. Rutherford, F. Ni, Proxy-based reconstructions of hemispheric and global surface temperature variations over the past two millennia. *Proc. Natl. Acad. Sci. U.S.A.* **105**, 13252–13257 (2008). Medline doi:10.1073/pnas.0805721105

28. A. Moberg, D. M. Sonechkin, K. Holmgren, N. M. Datsenko, W. Karlén, S.-E. Lauritzen, Highly variable Northern Hemisphere temperatures reconstructed from low- and high-resolution proxy data. *Nature* **433**, 613–617 (2005). Medline doi:10.1038/nature03265

29. T. M. Smith, R. W. Reynolds, T. C. Peterson, J. Lawrimore, Improvements to NOAA's historical merged land–ocean surface temperature analysis (1880–2006). *J. Clim.* **21**, 2283–2296 (2008). doi:10.1175/2007JCLI2100.1

30. A. J. Orsi, B. D. Cornuelle, J. P. Severinghaus, Little Ice Age cold interval in West Antarctica: Evidence from borehole temperature at the West Antarctic Ice Sheet (WAIS) Divide. *Geophys. Res. Lett.* **39**, 1–7 (2012).